Control of fine particles by time-averaged external forces in plasmas

doi: 10.1063/1.2353796

Control of fine particles by time-averaged external forces in plasmas

Satoru Iizuka, Kazuma Sakuta, Wataru Suzukawa, Kohgi Kato, and Takuma Gohda
Department of Electrical Engineering, Tohoku University, Sendai 980-8579, Japan

(Received 25 May 2006; accepted 18 August 2006; published online 5 October 2006)

A technique for the control of fine particle behavior is developed and demonstrated experimentally. In this method positive pulses are applied to two point-electrodes placed with some distance in plasmas containing fine particles. When the positive pulses are applied to these electrodes alternatively with a repetition period that is shorter than the particle response time, the particles feel only time-averaged force because of their large mass and are gradually transported toward the middle point between two point-electrodes wherever they are distributed initially. This method is quite effective for converging fine particles in the plasma. © *2006 American Institute of Physics*. [DOI: 10.1063/1.2353796]

I. INTRODUCTION

Fine particles of micron size in plasmas, charged negatively, are confined under the balance among electrostatic force, ion drag force, and gravitational force. Since the Coulomb-coupling parameter Γ is large, the particles reveal various characteristic behaviors concerned with a strongly coupled state.[1,2] In order to produce a three-dimensional Coulomb crystal the gravity gives an undesirable influence because of their large mass. On the earth the particles are inevitably trapped in the sheath with large potential gradient where ions are accelerated from the plasma, giving rise to a collective effect through the Coulomb collision with particles. For example, the particles are aligned in the vertical direction by the effect of the wake potential excited by the ion flow.[3,4] Therefore, an asymmetric Coulomb crystal is inevitably formed in the inhomogeneous sheath region. For this reason the experiment under the microgravity condition has been proposed and characteristic features of fine particles have been reported.[5–7] We have also clarified dynamic properties of fine particles under the microgravity condition.[8] In our previous experiments it was also demonstrated that the externally applied electric and magnetic fields drove a collective motion of particles.[9–11]

In a parallel plate rf discharge there frequently appeared a void in the fine-particle clouds.[12] The main reason is that the fine particles are pushed and transported by the ion drag force toward the plasma periphery where the outward-directing ion drag force balances with the electrostatic force directing inward. As a result, an empty region containing no fine particles, i.e., a void, is formed in the center of the particle clouds. Therefore, the elimination of the void is a crucial subject for investigating ideal three-dimensional Coulomb crystals in plasmas. In order to eliminate the void formation, we have proposed a production of low density plasma by a coaxially segmented radio-frequency (rf) electrode since the ion drag force is in proportional to the ion density of the plasma.[13] Another way to eliminate the void formation is to apply an external force, which is strong enough to cancel the outward-directing ion drag force.[14] These techniques are required to collect fine particles to form three-dimensional fine particle clouds in the plasma center.

In Sec. II we explain the principle of time-averaged particle driving (TAPD) method for control of the particle cloud in plasmas. The experimental apparatus and method are described in Sec. III. The experimental results and discussions are presented in Sec. IV. We finally conclude in Sec. V.

II. PRINCIPLE OF THE TAPD METHOD

Here, we propose a technique for a control of particle position by using a time-averaged particle driving (TAPD) method.[14] In this method time-varying forces acting on the fine particles, i.e., electrostatic force and ion drag force, are driven by a pair of point electrodes P_1 and P_2 introduced in the plasma as shown in Fig. 1. We apply positive pulse voltage alternatively to the point electrodes. When positive pulse is applied only to one of the point electrodes, P_1 for a period $T/2$, fine particles are accelerated toward P_1 by the force F_1.[15] However, as soon as they start to move, after a half period $T/2$, the pulse applied to P_1 is switched off. On the contrary, positive pulse is applied to the other point electrode P_2. Then, this moment the particles turn their motion toward P_2 by the force F_2. After the next half period $T/2$, the pulse applied to P_2 is switched off, while pulse application to P_1 is switched on again. In this way, the procedure is repeated continuously.

Because the particles have large mass, they feel only average force $\langle F \rangle$ if the repetition frequency is sufficient high. Namely, asymmetric force components in the x direction of F_1 and F_2 are almost cancelled to carry the particle toward the plane $x=0$, while force components in the y direction are added all the time to carry the particle toward the plane $y=0$. Here, the straight line connecting both point electrodes P_1 and P_2 is on the x axis. The origin $x=0$ is the middle point between P_1 and P_2. The straight line perpendicular to the x axis, passing through $x=0$ in a horizontal plane, is the y axis. Also the middle point between P_1 and P_2 is $y=0$. Finally, the particles are transported toward a middle point (0, 0) between P_1 and P_2, being independent of their initial positions. Here, x is in the P_1-P_2 direction as shown in Fig. 1(b). If we assume that the external force driven by P_1 and P_2 varies in time with frequency $\omega=2\pi/T$, then the amplitude of fine particle oscillation is given by $A=QE/M\omega^2$,

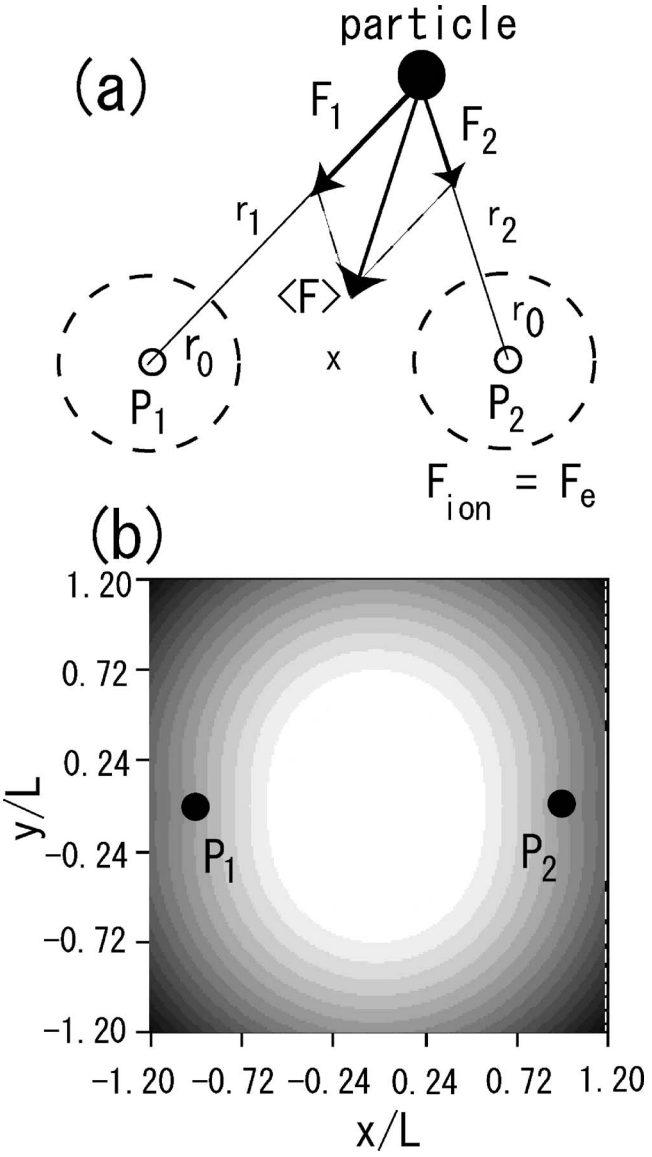

FIG. 1. A model of the TAPD method. (a) F_1 and F_2 are forces acting only time-interval 0-$T/2$ and $T/2$-T on particles at r_1 and r_2 from point electrodes $P_1(-L,0)$ and $P_2(L,0)$, respectively. T is pulse period, $\langle F\rangle$ is time averaged force F_1+F_2, r_0 is the position where ion drag force F_{ion} equals electric force F_e. (b) Contour plot of the equivalent potential Ψ in the horizontal x-y plane for $r_0/L=0.4$.

where Q is particle charge, M is particle mass, and E is electric field generated by the point electrodes. By employing fine particles of 10 μm in diameter, and using $QE\approx 1\times 10^{-12}$ N, $\omega/2\pi=100$ Hz, we obtain that A is a few μm which is much smaller than the interparticle spacing distance of 300 μm in our case. Therefore, we can observe an almost smooth motion of particles without any visible oscillation at ω.

The shape of the particle cloud in the final state can be estimated from the potential profile around the point electrodes. When positive bias voltage V_{b1} is applied only to P_1, the space potential ϕ in a plasma is not so affected as long as the voltage V_{b1}-ϕ does not exceed the ionization potential V_I, as usually seen for a tiny probe immersed in large plasmas. However, with increasing V_{b1} in the range V_{b1}-$\phi > V_I$, there may appear a local discharge around the tip of the point electrode P_1. Since a small plasma is turning on locally around the tip of P_1, ϕ in the background plasma is also influenced by V_{b1}. In this regime ϕ is pulled up in the whole plasma region by the increase in V_{b1}. Therefore, when fine particles are levitated in the plasma, the particles feel this potential increase wherever they are distributed initially. That is, almost all fine particles feel such potential variation and are accelerated toward P_1.

Here, we note that the forces acting on the fine particles are depending on the plasma density produced by the local discharge at the point electrode. In case of weak discharge, electrostatic force F_e directing toward P_1 is dominant. However, when the local plasma density is increased by the discharge at P_1, the ion drag force F_{ion} directing outward from P_1 overcomes F_e near the point electrode. However, leaving from the tip of the point electrode, F_{ion} decreases gradually due to the density decrease, and finally F_{ion} can be cancelled completely by F_e at $r=r_0$, i.e., $F_{\text{ion}}=F_e$, as shown by dotted circles in Fig. 1(a). Therefore, in the region $r_1>r_0$ the particles feel $\Delta F(=F_{\text{ion}}-F_e)$ (<0) directing toward P_1. On the other hand, the particles in $r_1<r_0$ feel ΔF (>0) directing outward. Here, r_1 is the particle distance from the point electrode P_1. If we restrict the particle motion near the point electrodes in the horizontal plane, the force in the r direction can be expanded by r around the position r_0. By neglecting the second and higher order dependency on r, the force can be approximately given by $\Delta\mathbf{F}_j=-\alpha(r_j-r_0)\hat{\mathbf{r}}_j$, where $r_j=|\mathbf{r}_j|$ is the distance from the point electrode P_j $(j=1$ and $2)$, $\hat{\mathbf{r}}_j$ is the unit vector parallel to $\mathbf{r}_j$, and α (>0) is constant depending on the plasma parameters. Therefore, the time-averaged force in the case of large ω is given by $\langle\mathbf{F}\rangle=\Delta\mathbf{F}_1+\Delta\mathbf{F}_2$ as shown in Fig. 1(a). Using the relation $\langle\mathbf{F}\rangle=-\nabla\psi$, we can obtain an equivalent potential ψ of the time-averaged force $\langle\mathbf{F}\rangle$. If we take the origin of the coordinates x and y at the middle point between $P_1(L,0)$ and $P_2(-L,0)$, then we obtain

$$\Psi(X,Y)\approx X^2+Y^2-R_0\left(\sqrt{(X-1)^2+Y^2}+\sqrt{(X+1)^2+Y^2}-2\right). \tag{1}$$

Here, we assume $\Psi(0,0)=0$. $X=x/L$, $Y=y/L$, $R_0=r_0/L$ (<1), $\Psi=\psi/\alpha L^2$. By expanding the second term around the origin, then we obtain

$$\frac{X^2}{\Psi}+\frac{Y^2}{\dfrac{\Psi}{1-R_0}}\approx 1. \tag{2}$$

Since $\Psi(\geq 0)$ becomes a minimum at (0, 0), the fine particles are trapped near the origin (0, 0) in an equivalent potential well Ψ with an ellipse shape. When $R_0=0$, the equivalent potential becomes a circle. Figure 1(b) shows the contour plot of Ψ for $R_0=0.4$. Therefore, it is expected that the fine particles are transported toward the minimum region of Ψ to form an ellipse-like particle cloud around the origin.

III. EXPERIMENTAL APPARATUS AND METHOD

The experiment is carried out inside a vacuum chamber that is 11.6-cm wide, 15-cm tall, and 11.6-cm long as shown

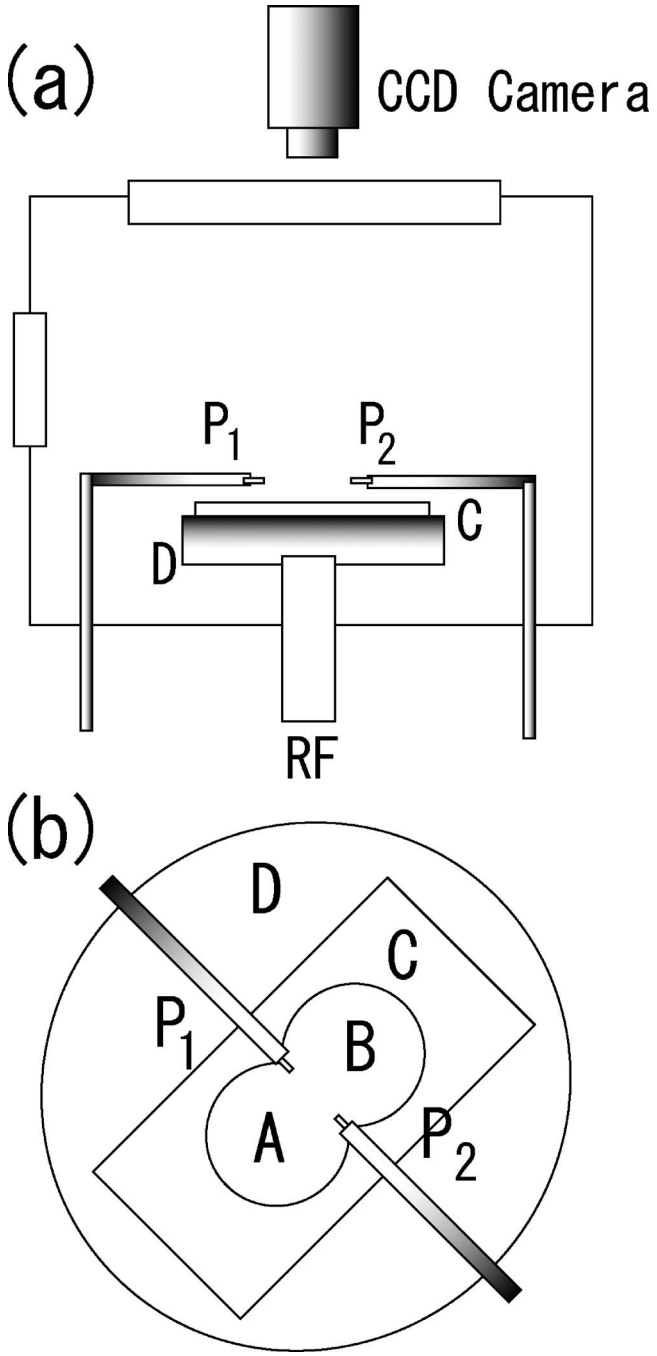

FIG. 2. (a) Experimental apparatus. P_1 and P_2 are point electrodes. Plate C is the levitation electrode, D is the rf electrode. (b) A and B are holes opened in the levitation electrode C placed on the rf electrode D. P_1 and P_2 are point electrodes.

in Fig. 2(a). The top and two sidewalls contain square view windows of 8 cm $\times$ 8 cm in length for laser beam injection and for observation of right-angle scattering from fine particles, respectively. The plasma is produced by a rf electrode of 10 cm in diameter placed at the bottom of the chamber. The rf power at 13.56 MHz, which can be changed up to 10 W, is applied to the electrode against a stainless-steel vacuum chamber which is grounded electrically. Argon gas is introduced at a fixed pressure of 20 Pa.

In order to confine the particles in a radial direction a levitation electrode plate C of 8 cm long $\times$ 4 cm wide and 1 mm thick is introduced on the rf electrode D to connect electrically with the rf electrode as shown in Fig. 2(b). The plate C contains one combined hole with circular regions A and B of 20 mm in diameter and 15 mm in the center distance. Fine particles used here are an acrylic sphere of 10 μm in diameter, which is dropped from the dust dispenser placed at 5 cm above the rf electrode. The dust dispenser can be movable in the radial direction, therefore it is drawn into a side port after injecting fine particles into the plasma. The particles are levitated at a few mm above the electrode. Usually, these particles form a monolayer dusty cloud.

For the control of fine particle positions two point electrodes P_1 and P_2 are introduced above the levitation electrode C, as shown in Fig. 2(a), at almost the same height as the fine particles to investigate simple motion of particles in the horizontal plane. The tip of the point electrode consists of a wire of 0.45 mm in diameter and 3 mm long. These electrodes are placed above the cross points of circular regions A and B as shown in Fig. 2(b). The distance between P_1 and P_2 is $2L=10$ mm. Low frequency positive pulse voltage with rectangular waveform is applied to the point electrodes alternatively. The repetition frequency can be changed within $\omega/2\pi=10-100$ Hz and the pulse voltage is fixed at $V_b=70$ V with a pulse duty of 50%.

IV. EXPERIMENTAL RESULTS AND DISCUSSIONS

We first investigate the effect of the point electrode biased at the dc-biased potential V_b. In the measurement of Fig. 3 we removed P_2. The Langmuir probe is shifted from P_1 to measure the spatial profiles. The current I_p and voltage V_b characteristics of the point electrode was observed. With an increase in V_b, the current I_p remarkably starts to increase at $V_b \approx 35$ V, indicating an appearance of local discharge at the tip of the point electrode. The floating potential V_f of the point electrode is about 0 V in the rf discharge. In order to investigate spatial profiles of plasma parameters we put a small movable Langmuir probe at x_p from the point electrode. Variations of space potential ϕ and electron density n_e are measured at every 1 or 2 mm and plotted as a function of x_p in Figs. 3(a) and 3(b), respectively. When the bias potential V_b is negative or floating potential V_f, the plasma potential near this point electrode is not much changed but almost uniform as shown in Fig. 3(a). However, with an increase in V_b the plasma potential changes drastically for $V_b > 37.5$ V. Since ϕ in the region far away from the pint electrode is not so much changed, there appears a potential gradient near the point electrode when $V_b > 37.5$ V.

When V_b is further increased, however, the plasma potential is increased drastically in the whole region, accompanied with a relatively large potential gradient near the point electrode. In the region far away from the point electrodes, the potential increases with V_b, although the spatial potential difference is not much changed. A weak potential gradient is still observed in regions A and B ($x_p \approx 10$ mm) even for larger V_b. Hence, the electric field directing outward is generated. We also observed that the increase in V_b is accompanied by a local plasma production due to the local discharge at the tip. For $V_b < 37.5$ V, the profile of the electron density

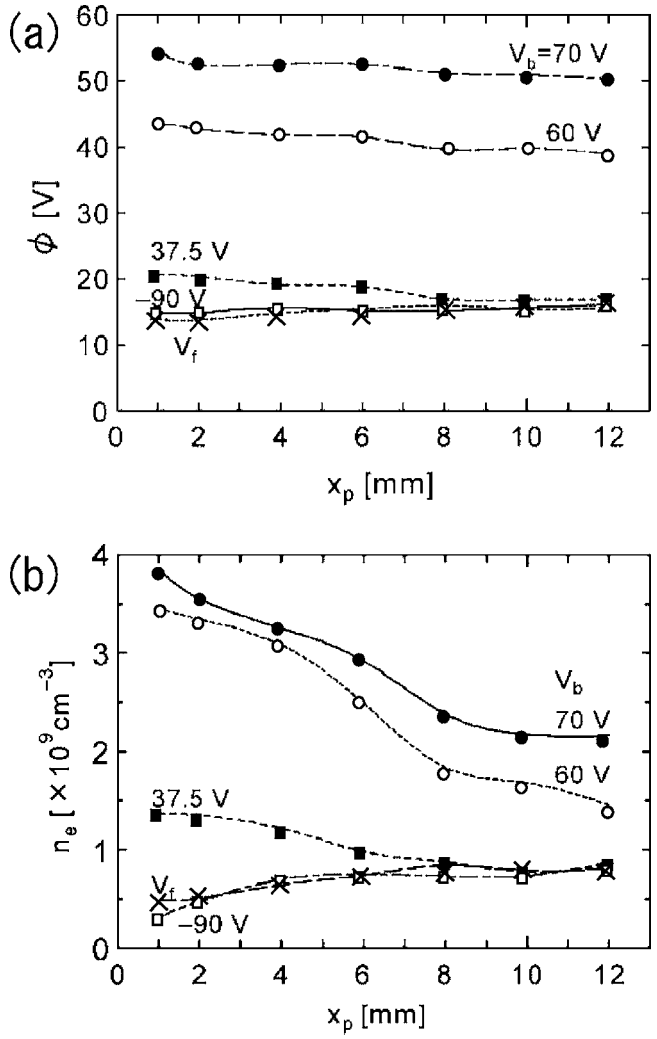

FIG. 3. Spatial profiles of (a) plasma potential ϕ and (b) electron density n_e as a function of x_p from the point electrode biased at potential V_b. V_f is the floating potential.

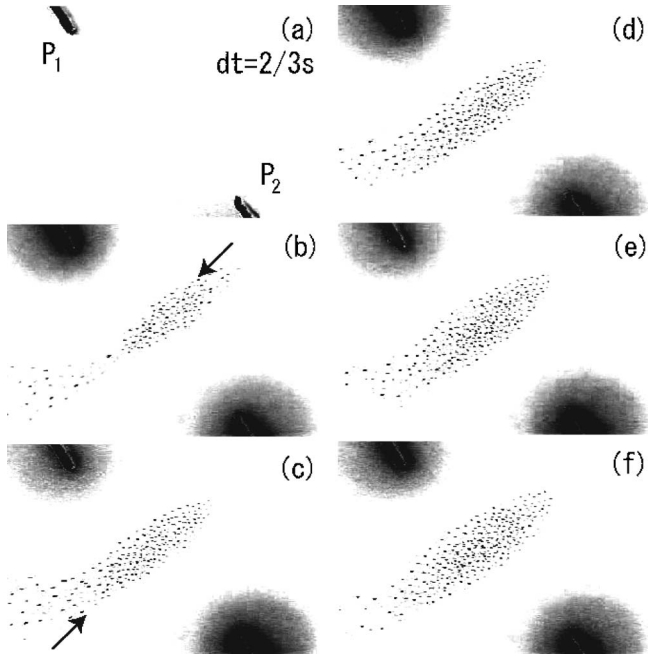

FIG. 4. Formation process of the particle cloud after pulse application to point electrodes P_1 and P_2. Arrows in (b) and (c) show the particles flowing from regions B and A shown in Fig. 2(b), respectively. Time interval is 2/3 s. Pulse frequency is 100 Hz and V_b is 70 V. Distance is $2L$ between P_1 and P_2 is 10 mm.

n_e is not changed. This is consistent with the result of the potential profile. However, n_e starts increasing locally around the point electrode for $V_b > 37.5$ V. When V_b is further increased, n_e increases in the whole region, accompanied with a steep density gradient near the point electrode. If n_e is increased near the point electrode, an ion drag force directing outward may appear to push the particles outward.

In case of the pulse-voltage application, the pulse duration time is extremely long compared with the time scales of plasma production and loss processes of the order of microseconds. Therefore, the time-averaged profiles can be simply obtained as an average of those of dc voltage ON and OFF, when the pulse duty is 50%. From potential profiles at $V_b = 60-70$ V in Fig. 3 we find not zero but a weak potential gradient even in the region $x_p \gg 1$ mm. The particles in regions A and B ($x_p \approx 10$ mm) far away from the point electrodes can feel this weak electric field even when the pulse voltage is applied, and are slowly and gradually driven toward the region between the point electrodes after many periods of pulses. The time-averaged potential in regions A and B will be also obtained from an average of those of dc voltage ON and OFF.

Particle response on the pulse application to the point electrodes is demonstrated in Fig. 4. The photos are taken at every 2/3 s. Before applying the pulse voltage V_p(=70 V) to the electrodes, the particles are mainly levitated above the center regions of A and B. Almost no particles exist near P_1 and P_2 as shown in Fig. 4(a). As soon as the pulse voltage is applied alternatively to P_1 and P_2 at a frequency of 100 Hz, we first observe a motion of particles coming from region B to the middle between P_1 and P_2 as shown by an arrow in Fig. 4(b). Note that since the photo is negative, dark spots around P_1 and P_2 show an appearance of bright discharge at the tips of P_1 and P_2. Then, this particle cloud is mixed with the particles coming from region A as shown by an arrow in Fig. 5(c). Although the particles move slowly from region A [Figs. 4(d)–4(f)], the particles finally construct a stationary particle cloud around the middle between P_1 and P_2 for $t \geq 4$ s as shown in Fig. 4(f).

The final steady state structure of the particle cloud is also shown in Fig. 5(b). The response time for the particle cloud formation is of the order of 1 s. As shown in Fig. 3, the potential far away from the point electrode ($x_p \approx 10$ mm) is almost unchanged when $V_b \approx 37.5$ V. However, with an increase in V_b, such potential increase spreads out in the radial direction. Then, the potential is increased in the whole region with a weak potential gradient at $x_p \gg 1$ mm. The particle response time, therefore, depends on V_b, although it may be saturated for larger V_b($\gg$37.5 V). When ω is decreased, we observe a large amplitude zig-zag motion of particles. The oscillation amplitude is increased with a decrease in ω. The particle motions at $\omega/2\pi = 10$ Hz and 100 Hz are shown in

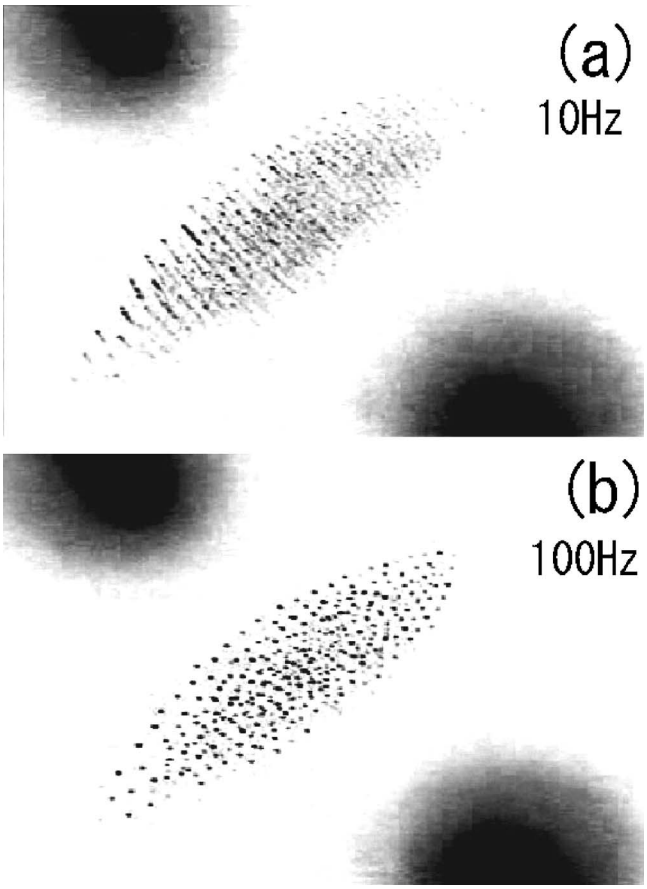

FIG. 5. Particle behaviors for the pulse frequency (a) 10 Hz and (b) 100 Hz. Other conditions are the same as in Fig. 5.

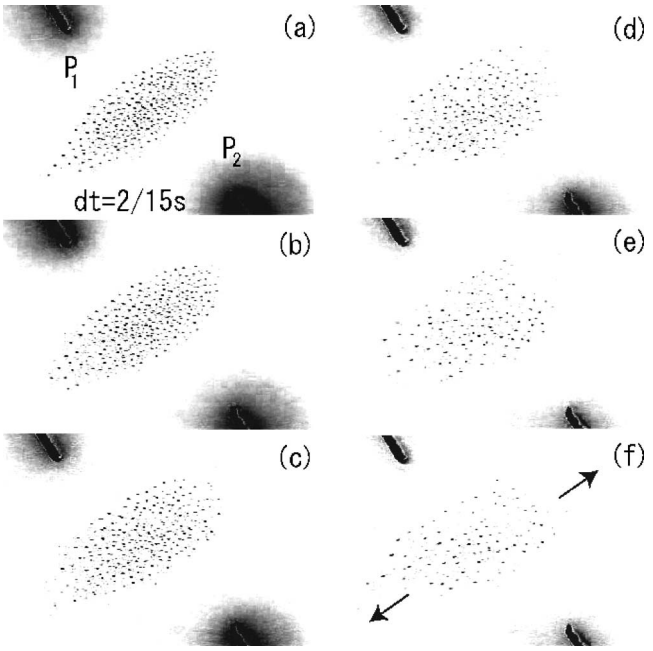

FIG. 6. Disruption process of particle cloud formed under the same conditions as in Fig. 5. Arrows in (f) show the particle flow toward regions A and B shown in Fig. 2(b). Time interval is 2/15 s.

Figs. 5(a) and 5(b), respectively. In the case of 10 Hz, we find orbits of particles oscillating along the electric field lines between P_1 and P_2. The amplitude of oscillation is a few times as much as the interparticle distance. On the other hand, in case of 100 Hz, we observe not particle oscillation but almost a stationary particle cloud, forming a Coulomb crystal. The width of the particle cloud in the x (P_1-P_2) direction is about 1/4 times as small as that in the perpendicular (y) direction, i.e., an ellipse-like structure is formed. A decrease in V_b makes the cloud more close to the circle. The final cloud shape is also affected by the zeroth order potential profile around the point electrodes. In our case, the cloud is stretched in the y direction. This is interpreted by a decrease in the time-averaged particle-collecting force in the y direction, because there exists more stable regions A and B for the particle levitation. This observed shape is consistent with the time-averaged potential shown in Fig. 1(b). The size of the particle cloud depends both on the distance between the electrodes and the number of particles supplied into the plasma. Under the finite gravity, the particles are distributed in the horizontal plane to form a two-dimensional (2D) particle cloud as shown in Fig. 5(b), where we find an ellipse-like particle cloud with a size of 2×8 mm in x and y directions, respectively, composed of a multishell structure like the onion near the surface and more dense crystallized bulk structure in the central region. The interparticle distance in the center region of the particle cloud is about 250 μm. Under the microgravity condition, however, the particles can distribute in the z direction perpendicular to the x-y plane to form three-dimensional (3D) crystals. The size of 3D particle crystals is also determined by the distance between the electrodes and the number of particles supplied into the plasma.

The disruption process of the particle cloud is shown in Fig. 6. The photos are taken at every 2/15 s. While turning off the pulses, the particle cloud expands a little bit as shown in Figs. 6(b) and 6(c). Then, the particles rapidly escape from the middle region between P_1 and P_2 toward the initial positions in A and B as shown by arrows in Fig. 6(f). Therefore, the particle density in the cloud quickly decreases in time and finally we cannot observe any particles between P_1 and P_2.

In our experiment, the particles are levitated above the levitation electrode C placed on the powered electrode D, which is used for capacitively coupled rf discharge as shown in Fig. 2. When the average plasma potential is raised up externally by the point electrodes, the powered electrode potential (i.e., self-bias voltage) will also vary, because of floating, to keep the rf input power constant. From the potential profile in Fig. 3, the particle height difference in the horizontal direction can be estimated from a simple sheath model. We get $\approx$0.1 mm for the self-bias voltage of 200 V. In fact, the height of the particles do not change when the positive pulse voltages are switched ON and OFF on the point electrodes as shown in Figs. 4 and 6.

The TAPD method developed here is quite effective for handling the charged particles produced in the processing plasmas. These particles are sometimes treated as contamination, which debase the quality of materials deposited. To date, several works have been reported on the dust removal from the processing plasmas.[16–18] However, all these works employed steady-state electric force, neutral drag force by

gas flow, and thermophoresis force by temperature gradient, which are intrinsically different from time-averaged particle driving force as in our paper. In the TAPD method, one pair of the point electrodes can act as tweezers, which can manipulate the particles one by one without mechanical direct contact.[19] We may apply this technique not only to the basic research of charged fine particles such as Coulomb crystal formation in plasmas but also to the transportation and elimination of particles from the processing plasmas.

V. CONCLUSIONS

We have demonstrated a control of particle position by using a new technique of the time-averaged particle driving (TAPD) method. Application of time-varying positive pulses to the point electrodes is quite effective for collecting particles in the middle between P_1 and P_2. The particles feel time-averaged force wherever they are placed initially, because the whole plasma potential is affected by the positively biased potential at the point electrodes when local discharge takes place at the tip. This method is quite important for transporting the particles to a fixed position in plasmas. We note that under the microgravity condition one pair of point electrodes would provide a spherical particle cloud in an equivalent spherical potential well ($X^2+Y^2+Z^2=\Psi$ in the limit $R_0=0$) produced by the TAPD method. This method is quite effective for creating a three-dimensionally (3D) asymmetric Coulomb crystal in the plasma center even when the void is created in the particle cloud.

The work was supported by a Grant-in-Aid for Scientific Research from the Ministry of Education, Culture, Sports, Science and Technology, Japan.

[1] S. Ichimaru, Rev. Mod. Phys. **54**, 1017 (1982).
[2] H. Ikezi, Phys. Fluids **29**, 1764 (1986).
[3] A. Melzer, V. A. Schweigert, and A. Piel, Phys. Rev. Lett. **83**, 3194 (1999).
[4] S. V. Vladiminov and A. A. Samarian, Phys. Rev. E **65**, 046416 (2002).
[5] G. E. Morfill, H. M. Thomas, U. Konopka, H. Rothermal, M. Zuzic, A. Ivlev, and J. Goree, Phys. Rev. Lett. **83**, 1598 (1999).
[6] O. S. Vanlina, A. P. Nefedov, O. F. Petrov, and V. E. Fortov, Phys. Rev. Lett. **88**, 035001 (2002).
[7] A. Ivlev, M. Kretschmer, M. Zuzic, G. E. Morfill, H. Rothermal, H. M. Thomas, V. E. Fortov, V. I. Molotkov, A. P. Nefedov, A. M. Lipaev, O. F. Petrov, Yu. M. Baturin, A. I. Ianov, and J. Goree, Phys. Rev. Lett. **90**, 055003 (2003).
[8] S. Iizuka, G. Uchida, S. Shimuzu, G. Nishimura, W. Suzukawa, and N. Sato, *Proceedings of the 23rd International Symposium on Space Technology and Science* (Society for Aeronautical and Space Science, Matsue, 2002), Vol. 2, p. 1724.
[9] G. Uchida, S. Iizuka, and N. Sato, IEEE Trans. Plasma Sci. **29**, 272 (2001).
[10] N. Sato, G. Uchida, T. Kaneko, S. Shimizu, and S. Iizuka, Phys. Plasmas **8**, 1786 (2001).
[11] S. Iizuka, M. Ozaki, and T. Gohda, Phys. Plasmas **11**, L5 (2004).
[12] G. E. Morfill and V. N. Tsytovich, Phys. Plasmas **9**, 4 (2002).
[13] W. Suzukawa, R. Ikada, Y. Tanaka, and S. Iizuka, Appl. Phys. Lett. **88**, 121503 (2006).
[14] S. Iizuka and K. Sakuta, Proceedings of the 12th International Congress on Plasma Physics, Nice, France, 2004, http://hal.ccsd.cnrs.fr/ccsd-00001785
[15] D. A. Law, W. H. Steel, B. M. Annaratone, and J. E. Allen, Phys. Rev. Lett. **80**, 4189 (1998).
[16] G. S. Selwyn, J. Singh, and R. S. Bennet, J. Vac. Sci. Technol. A **7**, 2758 (1988).
[17] G. M. Jellum, J. E. Daugherty, and D. B. Graves, J. Appl. Phys. **69**, 6923 (1991).
[18] Y. Kurimoto, N. Matsuda, G. Uchida, S. Iizuka, M. Suemitsu, and N. Sato, Thin Solid Films **457**, 285 (2004).
[19] S. Iizuka, K. Sakuta, W. Suzukawa, K. Kato, and T. Gohda, Thin Solid Films (in press).